Article:
Sullivan, RA, Davey, RJ, Sadiq, G et al. (5 more authors) (2014) Revealing the Roles of Desolvation and Molecular Self-Assembly in Crystal Nucleation from Solution: Benzoic and p -Aminobenzoic Acids. Crystal Growth and Design, 14 (5). pp. 2689-2696. ISSN 1528-7483

https://doi.org/10.1021/cg500441g

Revealing the roles of desolvation and molecular self-assembly in crystal nucleation from solution: benzoic and p-aminobenzoic acids.

R.A. Sullivan[1], R.J. Davey[1*], G. Sadiq[1], G. Dent[1], K. R. Back[1], J. H. ter Horst[2] , D.Toroz[3] and R. B. Hammond[3].

1. School of Chemical Engineering and Analytical Science, University of Manchester M13 9PL, UK; 2. Intensified Reaction & Separation Systems, Delft University of Technology, Delft, The Netherlands; 3 Institute of Particle Science and Engineering, University of Leeds, Leeds LS2 9J, UK

Abstract. There has been much recent interest in the role of solution chemistry and in particular the importance of molecular self-assembly in the nucleation of crystalline phases. Techniques such as FTIR and NMR have highlighted the existence of solution phase dimers which in many cases mirror the structural synthons found in the resulting macroscopic crystals. However there are no reported examples in which this new insight into the solution phase has been linked directly to the kinetics of crystal nucleation. Here for the first time, using a combination of solution FTIR, computational chemistry and measured crystal nucleation rate data, such a link is demonstrated for p-aminobenzoic (PABA) and benzoic acids nucleating from polar and nonpolar solvents. Solute dimerization and desolvation are found to be rate determining processes in the overall nucleation pathway.

Introduction.

Since the work of Volmer and Weber in 1926 (1) it has been appreciated that nucleation involves the dual processes of interface creation by molecular clustering and the attachment of molecules to clusters enabling their growth beyond a critical size (2). These phenomena may be thought of as respectively thermodynamic and kinetic in origin. There are many

examples in the literature in which the thermodynamic features of nucleation have been accessed by simple induction time measurements in order to estimate interfacial tensions and in their recent review Davey et al (3) have discussed how the underlying kinetic processes may be examined through full nucleation rate measurements. However, while in the past measurement of such kinetics has been experimentally demanding, the advent of high throughput experimentation techniques now offers a convenient route to the provision of increasing amounts of data with which to examine various aspects of the nucleation process. In the current study the Crystal16 induction time method is utilised (4, 5, 6) allowing the probabilistic nature of nucleation events to be properly quantified.

As an alternative to such kinetic measurements, recent work (3) has sought to examine structural links between solution species and structural synthons in the hope that new molecular level insights may be gained into the crystal nucleation process. The idea of a link between solution chemistry and nucleation was first suggested for 2,6-dihydroxybenzoic acid (7) on the basis of solubility data, spectroscopy, molecular modelling and the solid state chemistry of the known crystalline phases. Subsequent reports using NMR and FTIR (8, 9, 10, 11) supported a view that in solution intermolecular interactions can lead to the formation of supramolecular species that mirror the synthons present in the crystal structure. The detailed structural elucidation of supersaturated solutions using neutron scattering (12), has given detailed insight into the important role played by the solvent in stabilising the supersaturated state and highlighted the potential importance of solute desolvation in creating the molecular clusters that will become nuclei and crystals. These conclusions, however, are all based on studies of either the solution or the resulting macroscopic crystalline phase. To date there appear to have been no reports in which such insights into solution structure have been linked directly to the measured kinetics of nucleation. In the work reported here, therefore, we set out to combine measurement of nucleation kinetics, solubility, solution

FTIR data and computational studies with the aim of exploring, for the first time the links between the solution state of a molecule and its nucleation rate measured in a number of solvents.

This work formed part of a more general study of the model compound, p-aminobenzoic acid (PABA). This material has two enantiotropically related polymorphs, α and β (transition temperature 13.8 °C (13)) with known crystal structures (14, 15) and α the stable form above 13.8 °C. The α structure is based on the carboxylic acid $R_2^2(8)$ dimer (CSD refcode AMBNAC01) while that of β PABA comprises an H-bonded tetramer (CSD refcode AMBNAC04). The two forms have distinct needle and rhombic morphologies (16). Some additional experiments were also performed on benzoic acid which, like α PABA, crystallises in a dimer structure (17) but is not polymorphic.

Experimental.

PABA (≥99%), acetonitrile (≥99.5%), 2-propanol (anhydrous 99.5%) and ethyl acetate (≥ 99.5%), were purchased from Sigma Aldrich while benzoic acid (≥ 99.5%) and toluene (99.5%) were purchased from Fisher. All chemicals were used without further purification.

Nucleation rates were calculated using the probability method (4), from induction time distributions measured on a Crystal16, where all set temperatures of the Crystal16 were recalibrated to compensate for the inherent constant temperature difference between the measured temperature in the well and its set temperature. In acetonitrile and ethyl acetate a solution volume of 1.5mL was used, in 2-propanol 1.8mL and for benzoic acid in toluene 1mL. These volumes were found to be optimal for elimination of any unwanted formation ('crowning') of crystalline solids around the top of the solution vials. For each chosen supersaturation 120 mL of stock solution was made by dissolving the appropriate amount of α PABA in the respective solvents (for toluene / benzoic acid this was reduced to 50mL).

This stock solution was then dispensed into the Crystal16 vials each being heated to 40°C (50°C for benzoic acid), with constant magnetic stirring (900 rpm), for 30 minutes before cooling down to 20°C at a rate of 5°C/min. Attainment of the experimental temperature of 20°C (25°C for benzoic acid) was taken as time zero, after which the temperature was held constant for 8 hours. This cycle was repeated 5 times giving a maximum total of 80 induction time measurements at each chosen supersaturation. The induction time was taken as the difference in time between the decrease in optical transmission - indicative of nucleation – and time zero. Supersaturation ratios were calculated as $S=x/x^*$ with x as the supersaturated solution mole fraction of PABA or benzoic acid and x^* as the equilibrium solubility mole fraction. In order to check the form of PABA nucleated in these experiments, the solids nucleated at the lowest and highest supersaturation in each solvent were isolated immediately (within 1 minute) and characterised using both optical microscopy (Zeiss Axioplan 2 Microscope with Linksy software to capture and edit images) and powder X-Ray diffraction (Rigaku Miniflex benchtop XRPD machine in the Bragg-Brentano geometry with all powder samples scanned between 5° and 40° 2θ at a rate of 1.5° per minute with a step size of 0.03°). These experiments were supported by measurements of the transformation time of β to α PABA in which slurries of finely ground β crystals in the three solvents were held in the Crystal16 under the same conditions as in the nucleation experiments and sampled every hour to check for polymorph conversion. For each solvent two experiments were performed, with the mass of added β crystals calculated on the basis of the minimum and maximum supersaturations used in the induction time experiments.

Solubility data for α and β polymorphs has been reported previously (13, 16, 18, 19) but were re-measured in this work at 20°C for each solvent using a gravimetric method (five repeats). In order to check that no interconversion of forms took place during these experiments, solid phases present in the equilibrating slurries were characterised by powder XRD, optical

microscopy and FTIR spectroscopy. The latter were recorded (32 scans per spectrum; resolution 4 cm^{-1}) on an Avatar 360 ESP spectrometer with an ATR Golden Gate accessory and analysed with OMNIC software. Solution spectra were recorded using a Mettler Toledo ReactIR 4000 with a diamond composite ATR crystal (129 scans per sample from 4000 to 900cm^{-1} at 8 cm^{-1} resolution). The concentration ranges 0.39 - 0.0012M, 0.59M - 0.15M and 0.34M - 0.09M were explored for PABA solutions in acetonitrile, ethyl acetate and 2-propanol respectively, at 25°C.

Solvation free energies of PABA were calculated using the Thermodynamic Integration technique (TI) (20) at 293K and 1 atm in acetonitrile, 2-propanol and ethyl acetate. The technique was applied to compare the free energies of two non-interacting molecules with two molecules hydrogen bonded as an $R_2^2(8)$ carboxylic acid dimer. In the latter the dimer was maintained by use of a harmonic potential to define the atoms making up the two carboxylic acid groups. Each sampled PABA state was first minimised using the steepest descents method (21) and subsequently equilibrated for 100 ps. The initial state (λ=0) is defined by turning off the electrostatic and VDW interactions between the solute and the solvent. The final state (λ=1) is defined as having respectively the two non-interacting molecules and the carboxylic acid dimer fully solvated in a solvent box. Eight 'windows' were used for the integration pathway going from the initial to the final state $\Delta\lambda$= 0.0 0.2 0.4 0.6 0.7 0.8 0.9 1.0. For each window, further equilibration of the system was applied for 100 ps and sampled for 500 ps. All calculations were performed within the Gromacs programs package (22). Topology files, bonded and non-bonded parameters were derived from the GAFF force field (23). For the electrostatic potential, RESP charges were derived from Antechamber (24) within Ambertools based on ab-initio calculations at the MP2/aug-cc-pvTz level of theory.

Results.

Solubility.

Table 1 gives the saturation concentration of α and β PABA in the three solvents at 20°C together with that of benzoic acid in toluene, all measured in this work. As expected at 20°C, this being above the transition temperature, α PABA has the lower solubility. Reference values taken from the literature are also included and it is evident that our values compare well with previous measurements. The value of 0.089 g/g for α PABA (the stable form) in ethyl acetate reported by Gracin et al (16) appears to be in error, being larger than their quoted value of 0.087 g/g for β PABA. Referring to Table 1, it is clear that PABA is significantly more soluble in ethyl acetate than in acetonitrile and 2-propanol.

Solvent	**PABA α ($g/g_{solvent}$) Mole fraction**	**PABA β ($g/g_{solvent}$) Mole fraction**	**PABA Sol. Lit. values ($g/g_{solvent}$) Mole fraction**	
			α	**β**
Acetonitrile	0.060 (±0.001) 0.0176	0.0633(±0.0007) 0.0185	0.062 (18) 0.0182	0.063 (18) 0.0185
Ethyl acetate	0.0762(±0.0005) 0.0460	0.0770(±0.0005) 0.0471	0.089 (16) 0.0541 0.078 (18) 0.0478	0.087 (16) 0.0529 -
2-propanol	0.0615(±0.0005) 0.0265	0.0641 (±0.0023) 0.0326	0.067 (18) 0.0285	0.069 (18) 0.0292
Solvent	**Benzoic Acid ($g/g_{solvent}$) Mole fraction**		**Benzoic Acid Sol. Lit. values ($g/g_{solvent}$) Mole fraction**	
Toluene	0.104(±0.001) 0.073		0.107 0.075 (19)	

Table 1: The solubility of α and β PABA at 20°C and benzoic acid at 25°C measured in this work compared to literature data.

Infrared spectroscopy.

The solid state.

In the α PABA crystal structure the carbonyl group participates in hydrogen bonds which link molecules into classic carboxylic acid, $R_2^2(8)$, dimers. Half of these dimers are packed such that their carbonyl is involved in further H-bonds with adjacent -NH_2 groups which link alternate dimers (14). This gives rise to the α PABA crystal structure in which there are two molecules in the asymmetric unit, a feature reflected in the carbonyl stretching region of the solid state FTIR spectrum shown in Figure 1. The band at 1656 cm^{-1} is consistent with the asymmetric stretching vibrations of the hydrogen bonded carbonyl group. The additional strong band at 1622 cm^{-1}, represents the carbonyl groups of those acid dimers which also interact with –NH_2 groups. It is noted, but not shown, that there is a strong, broad absorption peaking at 930 cm^{-1} typical of the –O-H out of plane wag within a carboxylic acid dimer. (Nb. The bands in all three spectra of Figure 1 at ca 1636 cm^{-1} are likely overtone bands related to the phenyl ring.) Assignment of this solid state spectrum sets the scene for the interpretation of the major peaks present in the concentrated PABA solution spectra, seen in acetonitrile and 2-propanol also in Figure 1.

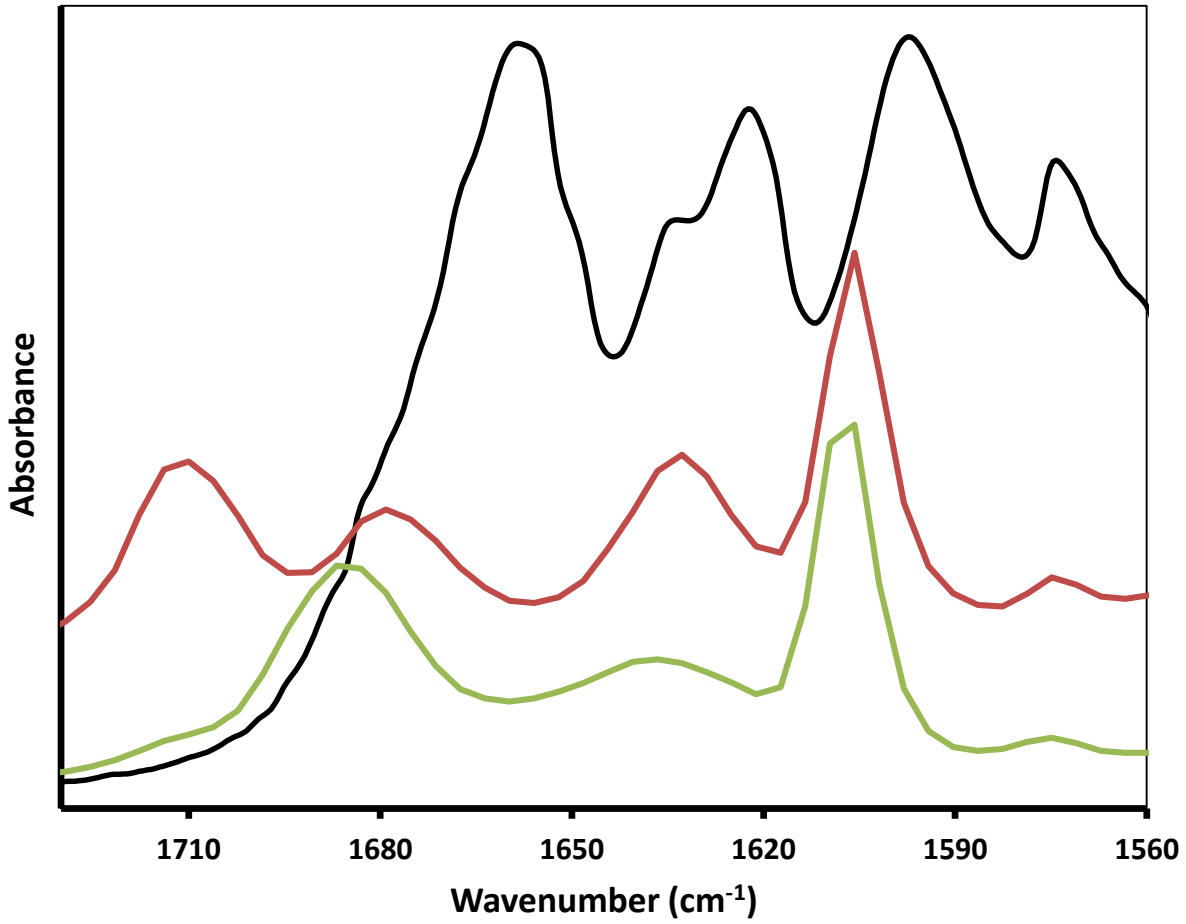

Figure 1: Solid state IR spectrum of α PABA (black) and solution spectra of saturated concentrations at 25°C of α PABA in acetonitrile 0.38M (0.071 g/g) (red) and 2-propanol 0.43M (0.076 g/g) (green).

The solution state.

The interpretation of the spectrum of 0.43M (0.076 g/g) PABA in 2-propanol (Figure 1) offers a convenient starting place. Given the solid state spectrum, it is evident that the strong band at 1685 cm^{-1} and the weaker band (shoulder) at 1715 cm^{-1} are both due to the carbonyl group, the former suggesting involvement in hydrogen bonding. The –OH wag region, around 940 cm^{-1} (not shown) is obscured by the solvent. Additional experiments with PABA and both benzoic and tetrolic acids (9) indicated that for all three molecules their carbonyl bands retain identical positions and relative intensities in both ethanol and methanol solutions. Hence, it seems reasonable to base an interpretation of these spectra on the detailed neutron scattering study of benzoic acid in methanol (12) which showed the carbonyl to

experience two possible interactions – one in which it is hydrogen bonded to a methanol OH group (-C=O…H distance ~ 1.6Å) and one in which it is hydrogen bonded to other benzoic acid molecules mainly via weak CH…O= interactions (~2.5Å). No evidence was found for acid dimers, even in supersaturated methanol solutions. On this basis therefore, the only reasonable assignment would be that the more intense peak at 1685 cm^{-1} relates to the solvated carbonyl while that at 1715 cm^{-1} arises from carbonyls in weakly self- associated (but not dimerised) molecules. This assignment is supported by the solid state FTIR spectra of both the β form of PABA (18) and the cocrystal of PABA with 4-nitropyridine N-oxide (25). In both structures the PABA carbonyl group is singly hydrogen bonded to an amino nitrogen, mirroring the solvation suggested here and the asymmetric stretches are at 1686 and 1680 cm^{-1} respectively, close to the value of 1685 cm^{-1} seen in 2-propanol solutions.

In the spectrum of 0.38M (0.071 g/g) PABA in acetonitrile in Figure 1 there are also two carbonyl bands (1710 and 1683 cm^{-1}) but with intensities reversed compared to the 2-propanol solution. In this case the solvent contains no H-bond donor and so the carbonyl will not be strongly solvated. It seems most likely that in this case the more intense band at 1710 cm^{-1} is due to weakly solvated carbonyl groups and the less intense band at 1683 cm^{-1} to hydrogen bonded interactions with other solute molecules. Whether or not such solute-solute interactions take the form of dimers is unclear –acetonitrile has a strong, sharp band at 919 cm^{-1} which appears unchanged in PABA solutions. Given the solid state spectrum of α PABA, the existence of dimers in solution might be expected to result in a broad shoulder on the higher wavenumber side of this adsorption. This is not evident and hence we are inclined to the view that there are no dimers present, their formation being hindered by solvation of the –OH group by acetonitrile. Upon dilution of these solutions to 0.0012M the band positions do not shift to higher wavenumbers, further supporting the view that solvated monomers exist even in concentrated acetonitrile PABA solutions. In ethyl acetate solutions

(spectrum not shown) the asymmetric carbonyl stretching bands are obscured by the solvent and thus could not be resolved reliably. However, there is a shoulder around 1700-1710 cm^{-1} implying behaviour similar to acetonitrile, with strong solvation of the hydroxyl group preventing the formation of acid dimers in solution.

As an adjunct to experiments in these polar solvents it was thought desirable to perform nucleation experiments in a solvent in which solute dimers would definitely be present. Because PABA is essentially insoluble in all non-polar solvents this proved impossible and so, as a convenient alternative benzoic acid in toluene was studied. This acid is known to be dimerised in both the solid state and in non-polar solvents (9). In previous work Davey et al (9) reported that in its dimer based crystal structure the asymmetric carbonyl stretch appears at 1684 cm^{-1} and the -OH wag at 935 cm^{-1}. For benzoic acid in toluene, these bands fall at 1694 cm^{-1} and 938 cm^{-1} respectively giving a clear indication of dimerisation in these solutions.

Figure 2 provides a schematic summary of the solvation interactions of PABA and benzoic acid in solution. Figure 2a shows the solvation of both acid carbonyl and hydroxyl groups by 2-propanol (12), while Figure 2b and c show the hydrogen bonded interaction between the acid hydroxyl and acetonitrile and ethyl acetate. Finally Figure 2d shows both the self-assembled benzoic acid dimer and its solvation via π-π interactions with toluene.

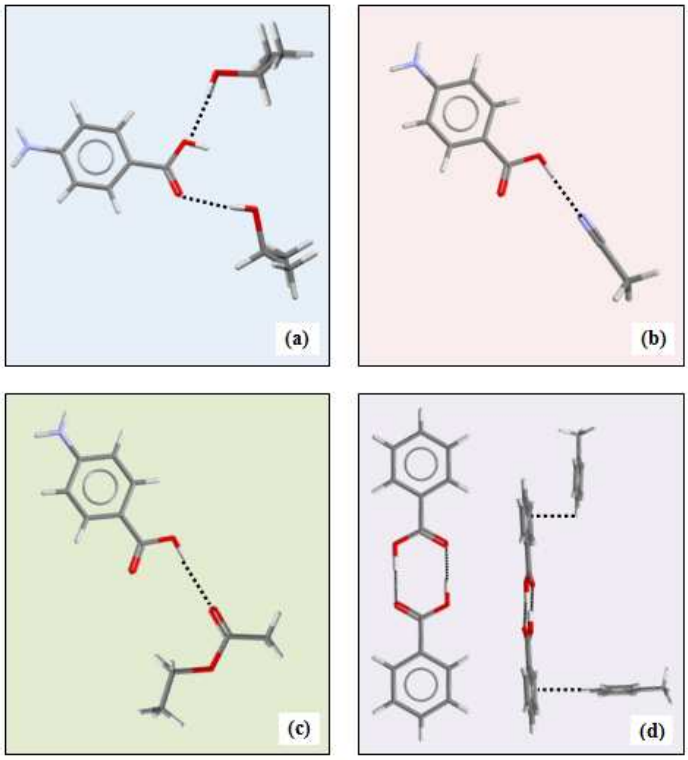

Figure 2: Schematic illustration of solvation interactions in solution of PABA in (a) 2-propanol, (b) acetonitrile, (c) ethyl acetate and (d) benzoic acid in toluene.

Molecular dynamics calculations.

The calculated solvation free energies of PABA species are listed in Table 2. In comparing the free energies per mole of two non-interacting PABA molecules with that of PABA dimers we are essentially looking at the relative stabilities of solvated and non-solvated (dimerised) acid groups and in this sense the calculation reflects the change that must occur on nucleation from solvents in which the solute is essentially totally solvated. Overall it is clear that in 2-propanol two isolated molecules of PABA are strongly preferred (ca.+11kJmol^{-1}) over the carboxylic acid dimer, in ethyl acetate the situation is more finely balanced with monomers favoured by only ca. +0.3kJmol^{-1} whilst in acetonitrile the difference is ca.-5kJmol^{-1} in favour of dimers. If desolvation were the rate determining step in dimer formation it might be expected on this basis that nucleation would be slowest from 2-propanol and fastest from acetonitrile.

Solvent	Solute Species and its Free Energy of Solvation (kJmol^{-1})		
	Two isolated monomers	**Carboxylic acid Dimer**	**ΔΔG**
Acetonitrile	-90.14 +/- 1.23	-95.82 +/- 1.75	-4.68
Ethyl acetate	-102.13 +/- 1.96	-101.86 +/- 1.84	+0.27
IPA	-95.10 +/- 1.72	-84.34 +/- 1.61	+10.96

Table 2: Calculated solvation free energies of the carboxylic acid dimer and two distinct monomers of PABA in acetonitrile, ethyl acetate and 2-propanol, at 293K and 1 atm.

Induction time measurements.

Because PABA is an enantiotropic dimorphic system all the compositions used for the induction time measurements produced solutions supersaturated with respect to both phases. However, the form nucleated and isolated within 1 minute was always α PABA. In the separate polymorph conversion experiments, it was found that slurries of β in all solvents took in excess of 2 hours for the first α crystals to appear. Thus for the α PABA detected in the induction time experiments to have originated from β, these β crystals would have had to nucleate and totally transform in less than 1 minute. These results suggest that this is highly unlikely and confirms that if the β form had appeared it would have been detected. It is thus evident that the nucleation kinetics reported here are those of the α-form and that this material does not follow Ostwald's Rule.

Figure 3 shows the probability distribution obtained for the measured induction times of α PABA in acetonitrile at 20°C. These data were fitted to equation 1 (Origin 8.0) in order to derive nucleation rates. A key parameter in this analysis is the growth time, t_g, accounting for the delay in detection arising from growth (4). For a given supersaturation this time was taken as the minimum time required for induction to be observed. As the supersaturation increases,

the probability P(t) more rapidly approaches 1, indicating higher nucleation rates. For example the derived rates, J, for supersaturation ratios, S, of 1.08, 1.10, 1.12, 1.14, 1.16 and 1.20 were 8, 90, 171, 307, 413 and 662 $m^{-3}s^{-1}$. Given that the chosen methodology allows for excellent control over temperature, volume and composition, the observed spread of probability of induction (Figure 3 and in references 4, 5, 6) effectively illustrates the stochastic nature of nucleation. Probability distributions of measured induction times for α PABA at 20 °C in 2-propanol and ethyl acetate can be found in the additional information.

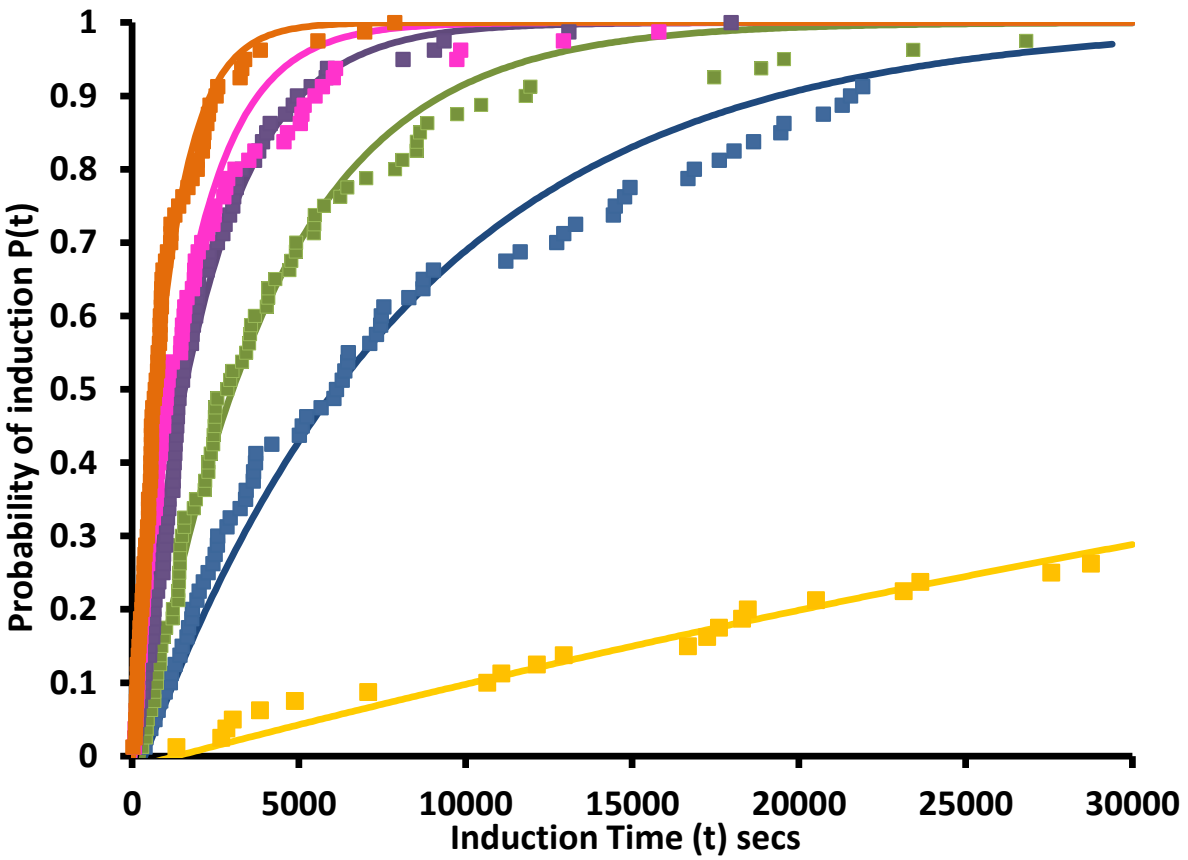

Figure 3: Experimentally obtained probability distributions P(t) of the induction times measured at 1.08 (yellow), 1.10 (blue), 1.12 (green), 1.14 (purple), 1.16 (pink) and 1.20 (orange) supersaturation ratio for α PABA in acetonitrile at 20°C, with solid lines being fits of equation 1 to the experimental data and t_g fixed as the fastest induction time per supersaturation ratio measured.

According to classical nucleation theory the dependence of nucleation rate on supersaturation is described by equation 2. Thus, the nucleation rates obtained can be plotted (Excel) using

the linear function of $\ln(J/S\ln^2 S)$ versus $1/\ln^2 S$ to derive the pre-exponential kinetic factor A_0 from the intercept and the thermodynamic parameter B from the gradient. These linear fits are shown for each solvent in Figure 4.

$$P(t) = 1 - \exp(-JV(t - t_g)) \quad \text{Equation 1}$$

$$J = A_0 S \ln^2 S \exp(-\frac{B}{\ln^2 S}) \quad \text{Equation 2}$$

From the parameter A_0, information about the molecular kinetics of the nucleation process can be obtained through derived values of f^*C_o, the product of f^*, the attachment frequency of building units to a nucleus and C_o the concentration of nucleation sites, as defined in equation 3.

$$A_0 S \ln^2 S = z f^* C_0 \quad \text{Equation 3}$$

where z is the Zeldovich factor derived and calculated according to Kashchiev ((2) in equation 13.36, chapter 13). In experiments of the type performed here nucleation occurs heterogeneously at undefined surfaces and hence the true value of C_o is unknown. However, given that these data were acquired using the same experimental procedure and in the same laboratory it seems reasonable to assume that estimated values of f^*C_o may at least be used to infer the relative rates of molecular attachment during nucleation from different solvents or of different solutes. Further to this and following equation 5 in reference 3 this attachment frequency is also a linear function of the concentration of building units in solution and hence such comparisons should be made via values of f^*C_o/M in which M is the solution molarity. As discussed below, these values for different solvents then reflect the effectiveness of the respective solution associates in determining the nucleation rates.

The thermodynamic parameter B, is defined in equation 4, where, c is the shape factor [$(36\pi)^{1/3}$ for spherical nuclei] (4, 26), v is the molecular volume of the crystalline phase, γ_{eff} is

the effective interfacial tension, k is the Boltzmann constant and T the absolute temperature. From this relationship we can obtain information about the free energy barrier associated with the formation of nuclei from solution through calculated values of γ_{eff} in each solvent.

$$B = -\frac{4}{27}\frac{(c^3\nu^3\gamma_{eff}^3)}{(k^3T^3)}$$ Equation 4

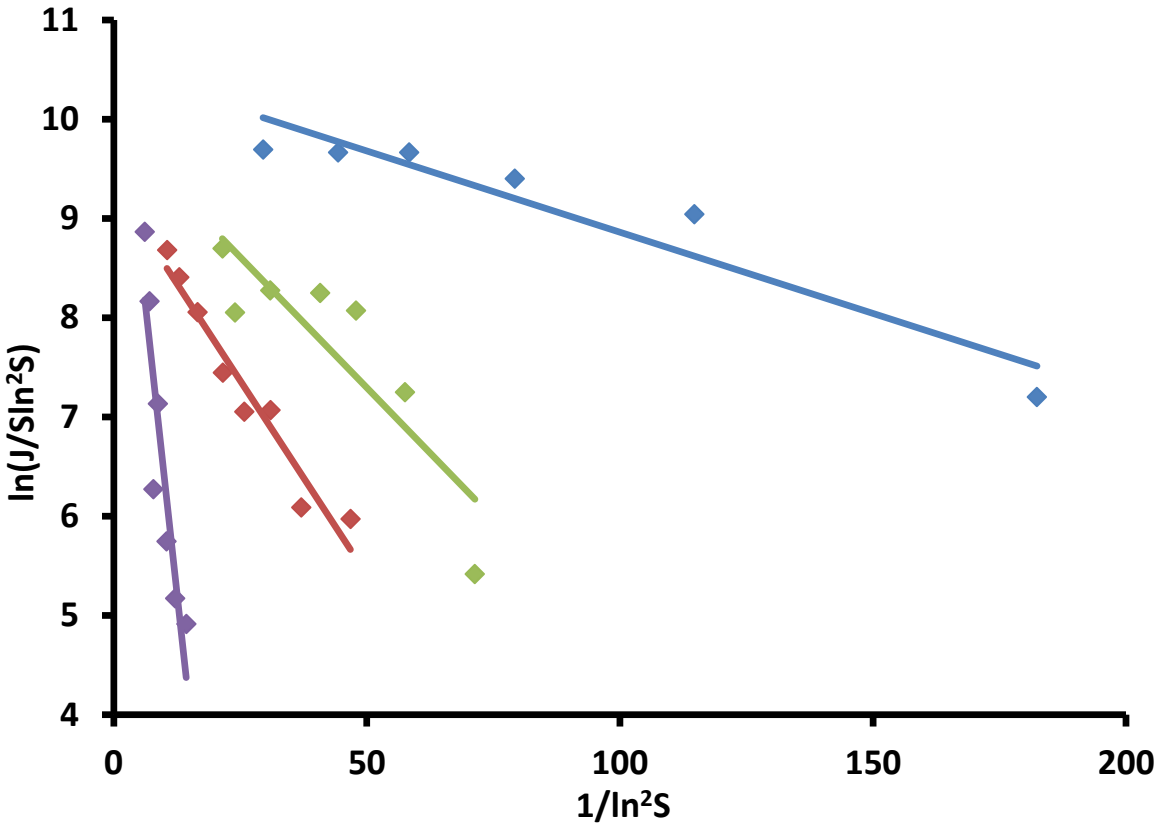

Figure 4: Plot of ln(J/Sln^{2}S) as a function of 1/ln^{2}S for α PABA at 20 ºC in acetonitrile (red), (R^2 = 0.91), ethyl acetate (green), (R^2 = 0.76), 2-propanol (blue), (R^2 = 0.95) and benzoic acid at 25 ºC in toluene (purple), (R^2 = 0.82).

Table 3 lists the values of A and B obtained for PABA in the three solvents and benzoic acid in toluene. Benzoic acid in toluene has the largest kinetic parameter followed by α PABA in acetonitrile, then ethyl acetate and finally the smallest kinetic parameter is α PABA in 2-propanol with a value of 1.09x10^4 m^{-3}s^{-1}. The effective interfacial tension values, γ_{eff}, are also detailed in Table 3 and indicate that with respect to α PABA most energy is spent creating

interface in 2-propanol, with γ_{eff} at 2.24 mJm^{-2}, followed by ethyl acetate and finally acetonitrile. Overall it is energetically most costly for benzoic acid in toluene. This trend is reflected in Figure 5, where the critical nucleus size for PABA in each solvent is charted over a range of supersaturations: for higher γ_{eff} values a higher supersaturation is needed to reach the same critical nucleus size.

Solute	Solvent	A_0 ($m^{-3}s^{-1}$)	B	γ_{eff} (mJm^{-2})
PABA	Acetonitrile	3.63×10^4	0.016	1.33
PABA	Ethyl acetate	2.05×10^4	0.053	1.96
PABA	2-propanol	1.09×10^4	0.078	2.24
Benzoic acid	Toluene	6.18×10^4	0.46	4.34

Table 3: Values of derived parameters A_0, B and γ_{eff} for α PABA in, acetonitrile, ethyl acetate, 2-propanol, and for benzoic acid in toluene.

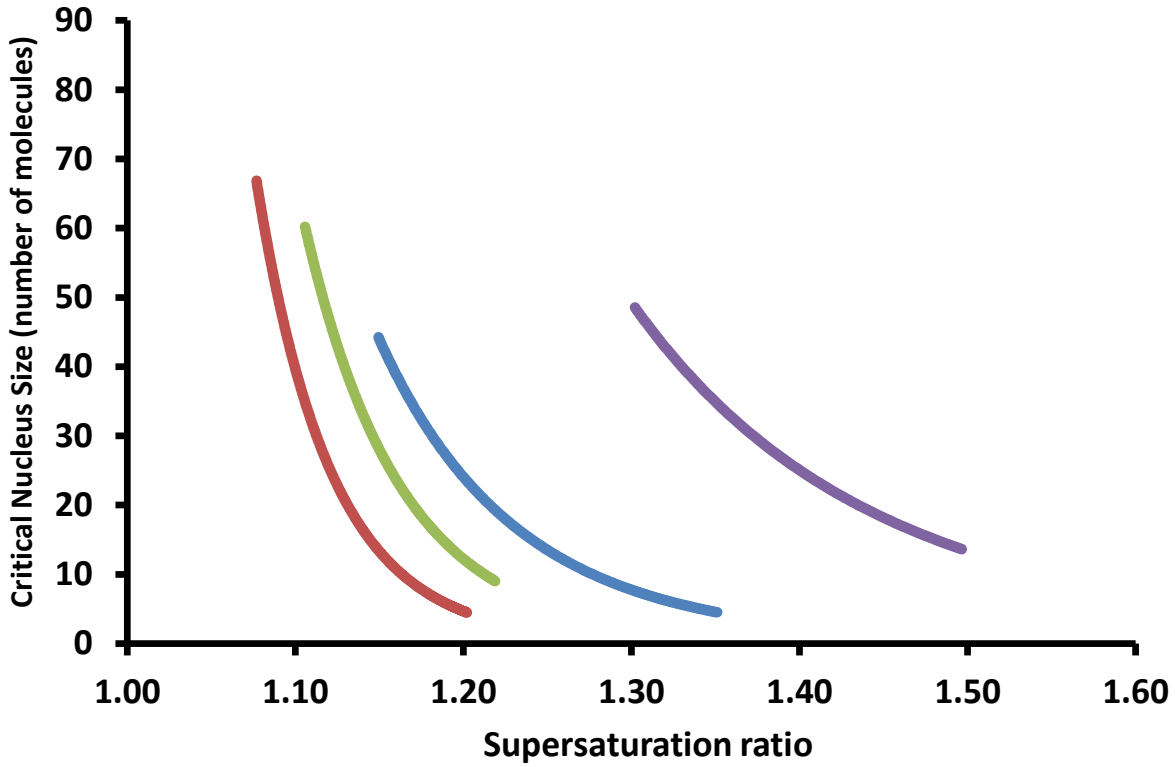

Figure 5: The critical nucleus sizes ($n^*=2B/\ln^3 S$) for α PABA over a range of supersaturations at 20 °C in acetonitrile (red), ethyl acetate (green), 2-propanol (blue) and benzoic acid in toluene (purple) at 25 °C.

Using the derived kinetic parameters for PABA and benzoic acid f^*C_o/M was calculated and Figure 6 shows how this varies with supersaturation, solvent and solute. Clearly, benzoic acid in toluene has faster relative rates of molecular attachment by almost an order of magnitude in comparison to α PABA in any of the solvents chosen. For α PABA, molecules have the fastest relative rate of attachment in acetonitrile followed by ethyl acetate with 2-propanol the slowest. Given these data it is now possible to explore the link between the molecular processes controlling nucleation and the nature of the solution phase interactions discussed above.

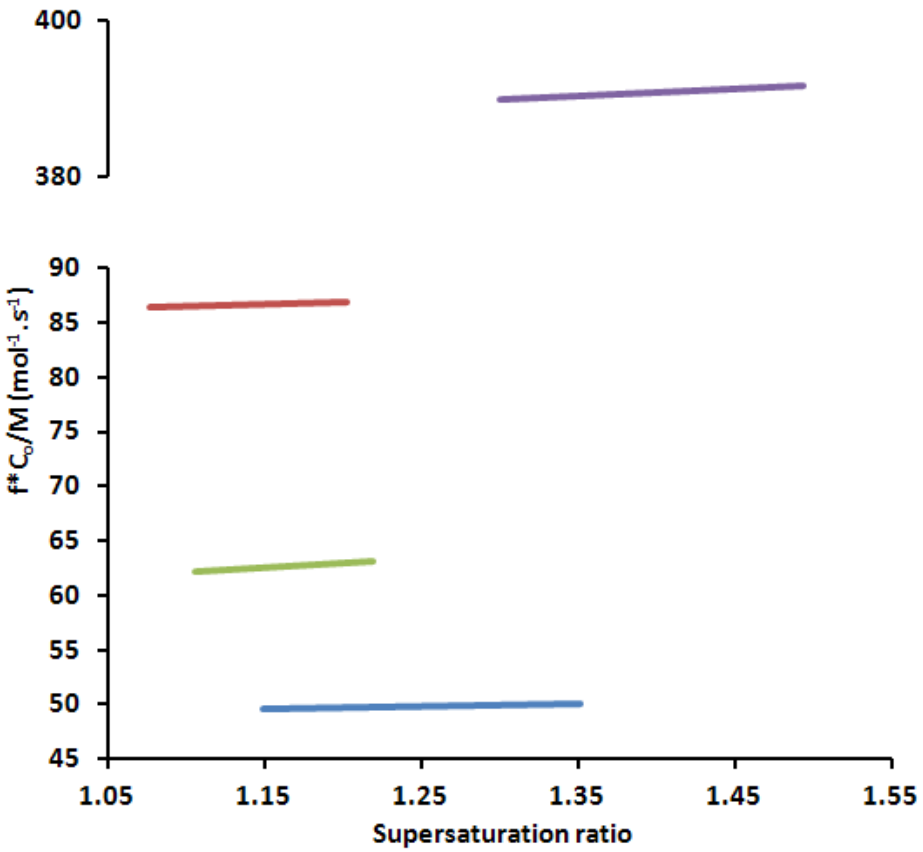

Figure 6: The dependence of f^*C_o/M ($mol^{-1}.s^{-1}$) on the supersaturation ratio for α PABA at 20°C in 2-propanol (blue), ethyl acetate (green) and acetonitrile (red) and benzoic acid at 25°C in toluene (purple).

Discussion & Conclusions.

Firstly it is noted that the appearance of α PABA throughout this work is in good agreement with other recent studies. For example, Gracin and Rasmuson (16) reported that, for a range of organic solvents, α PABA was the kinetically favoured form: primary nucleation of β PABA was only achieved by very slow cooling of ethyl acetate solutions saturated at temperatures below 15°C. Svard et al (18) reported that in 330 experiments in which solutions of PABA saturated at 15, 20, 30°C in methanol, acetonitrile and ethyl acetate were subsequently cooled, α PABA was again the only form isolated. In attempting to understand why the nucleation of the β form is so difficult, these two reports came to contradictory conclusions. The former hypothesised that dimerization in solution led to the formation of the dimer based α polymorph while the latter acknowledged that PABA would be solvated and hence the solutions would probably not contain dimers. Certainly it is known that both scenarios can be true for carboxylic acid crystallisation (9) however, this previous work (16) provided no experimental evidence for the state of the PABA carboxylic acid group in the solvents used.

The new data reported here combine for the first time experimental evidence of the solvation state of PABA (Figure 2), computation of the relative free energies of dimer formation (Table 2) and nucleation kinetics (Figure 6). It is now possible to examine more fully the links between solvation, self-assembly and the nucleation process. Of the three solvents studied it has been concluded that the carboxylic acid groups in PABA are most strongly solvated by 2-propanol. For the acid groups of two PABA molecules to form a dimer, two H-bonded propanol molecules must be removed from each, requiring the breakage of 4 hydrogen bonds. Acetonitrile and ethyl acetate, having no H-bond donors provide less effective solvation with only two solvent molecules to be removed to enable dimer formation. The

more detailed calculation revealed through the MD results of Table 2 verify this situation, confirming 2-propanol as the solvent in which dimers compare least favourably with monomers. These calculations also suggest subtle differences between ethyl acetate and acetonitrile with relative stability of dimers and monomers increasingly favouring dimers in the latter. If this relative stability of monomers and dimers is compared to the relative attachment frequencies estimated from the nucleation rates (Figure 6) it is evident that there is a good correlation in which the lowest rate is observed in 2-propanol, the strongest solvator of the carboxylic acid group with rates increasing for the weaker solvators, ethyl acetate and acetonitrile in line with the ΔΔG values of Table 2. So for example at a supersaturation ratio of 1.15, the relative values of $f^*.C_o/M$ in 2-propanol, ethyl acetate and acetonitrile are 1, 1.26, 1.74.

It is now possible to draw two important conclusions. Firstly these relative rates do not correlate with the magnitude of the relevant solubilities (Table 1) which are highest in ethyl acetate and lower in both acetonitrile and 2-propanol. Secondly the rates do correlate with the free energies of specific desolvation of the carboxylic acid group and formation of the acid dimer. This suggests that the rate determining step in cluster growth during nucleation is not the overall desolvation of PABA involving breakage of both H-bonds and non-specific van der Waals contacts but rather the specific desolvation of the carboxylic acid group leading to the creation of the $R_2^2(8)$ acid dimer.

If, in accordance with classical nucleation theory, molecular clusters are assumed to have the packing and morphology of a mature α- crystal then further elaboration of this mechanism is possible. Macroscopic α- crystals comprise b-axis needles in which the fast growth direction is associated with π-π stacking interactions, the ease of formation of which will be essentially independent of solvent. However, it is growth of faces in the [010] zone that are slowest and

rate limiting and these are the very surfaces ({002} and {-101}) at which desolvation of the carboxylic acid groups lead to the formation of the acid dimer, the key structural synthon. It is thus concluded that indeed the overall process of transforming a molecule from solution to cluster is controlled by desolvation and dimer formation.

It was by way of a further test of this conclusion that experiments were performed on benzoic acid nucleating in toluene. In this case, as discussed above, self-assembled $R_2^2(8)$ benzoic acid dimers already exist in solution and hence their formation need not take place during nucleation thus making the desolvation enthalpy effectively zero compared to PABA. If indeed desolvation and dimer formation do control the molecular attachment frequency then a much higher rate would be expected for benzoic acid in toluene than for PABA in polar solvents. As seen in Figure 6 this indeed turns out to be the case with the relative value of f^*C_o/M at a supersaturation of 1.15 being 7.82, almost an order of magnitude higher than the PABA values. These conclusions are further reinforced by a similar trend in the relative values of the derived interfacial tensions and the critical radii (Table 3 and Figure 5).

Overall these appear to be very significant results in advancing our understanding of the key factors controlling nucleation rates. The attachment kinetics of PABA molecules to growing nuclei are dominated by the processes of desolvation and acid dimer formation; solution phase self-assembly of such dimers (as in benzoic acid) can lead to an order of magnitude enhancement in the nucleation rate. To our knowledge, this is the first time that a direct link has been made between nucleation kinetics and molecular processes occurring in solution. in The scheme in Figure 7 shows these two distinct pathways to the nucleus, one involving direct addition of self-assembled dimers (viz. benzoic acid) and the other requiring desolvation of both surface and solution phases acid groups (viz. PABA).

In revisiting previous studies in which the nucleation kinetics have been measured in different solvents the only work available appears to be the 1957 report from Dunning and Notley (27) who measured the nucleation kinetics of cyclonite from acetone-water mixtures. Reanalysis of their data gives values of f^*C_0/M in the range 10^9 to 10^{11} $m^{-3}s^{-1}$. These values are significantly higher than for PABA and are to be viewed with caution since cyclonite is polymorphic (28), a factor unknown at the time. Never the less, following our arguments regarding PABA these higher values are consistent with the likely weak solvation of cyclonite by acetone and water. More recently ter Horst et al have reported data for the nucleation of isonicotinamide (6) from the single solvent, ethanol. Using these data f^*C_0/M is

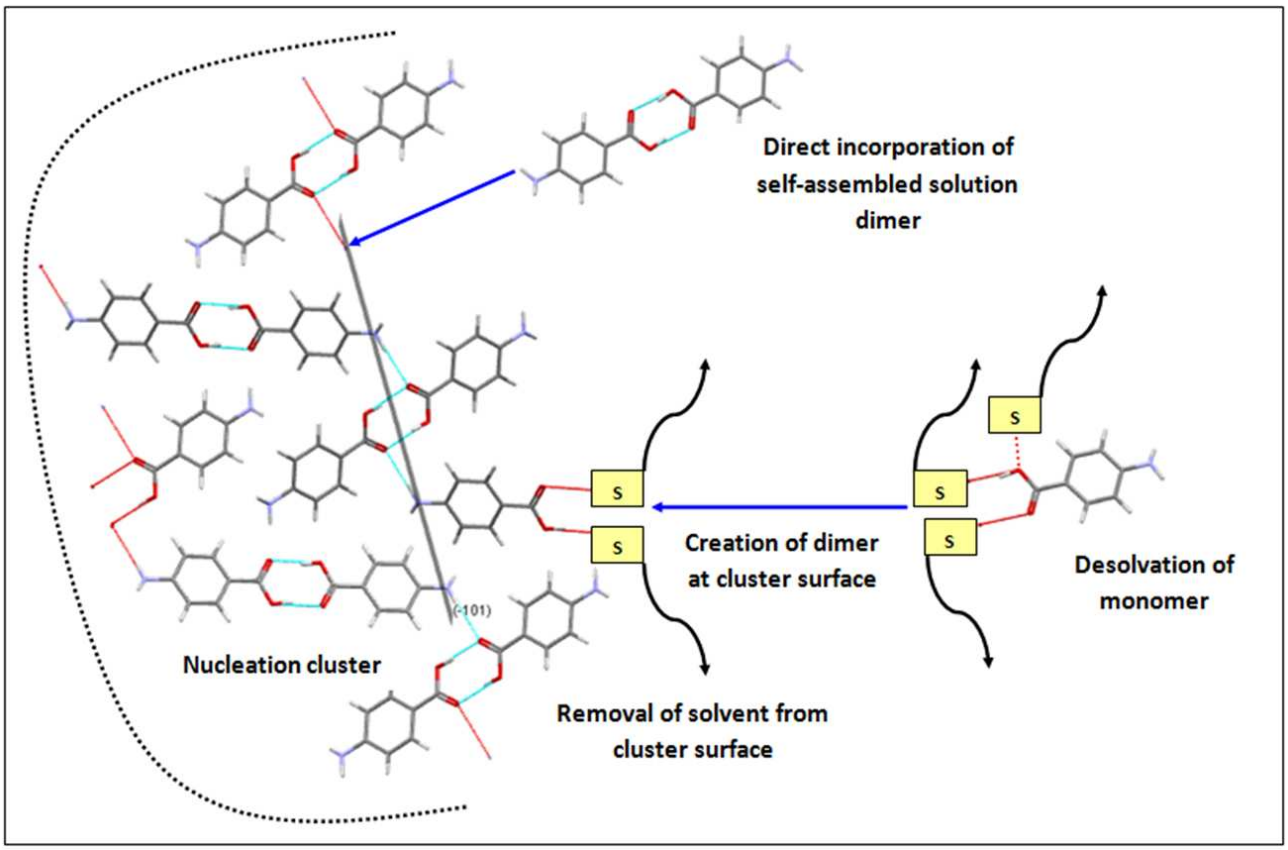

Figure 7: A schematic illustration contrasting the nucleation pathway of self- assembled dimers with that of solvated monomers. Growth units are shown joining a (-101) surface.

estimated here to be about $60x10^3$ m^3s^{-1}. Given the likely solvation in solution (10) this value seems to be consistent with our current values for PABA.

Overall this work indicates the vital role played by pre-assembly and desolvation in the nucleation process. It clearly supports the results of previous work on solution chemistry and in particular neutron scattering studies of methanolic benzoic acid and aqueous solutions of urea and hexamethylenetetramine (3). Here not only did solvation appear to stabilise the supersaturated state but also the solute-solute co-ordination in solution was shown to reflect many of the elements of the crystal structures with only solvent removal hindering the densification to the known crystal packing.

Of course, we are well aware that the conclusions drawn from these data rely on the concepts of classical nucleation theory. While no attempt is made to justify this, it has to be said that it leads to a result of compelling simplicity, offering an intellectually satisfying interpretation of the data.

Acknowledgements. RAS, RJD, DT and RBH were funded through the EPSRC 'Critical Mass' programme.

References

1. M. Volmer, A. Weber, Zeitschrift für Physikadische Chemie. **1926,** 119, 277-292.
2. D. Kashchiev, Nucleation: Basic Theory with Applications, Butterworth Heinemann, Oxford, **2000.**
3. R. Davey, S. L. M. Schroeder, J. H. ter Horst, Angew. Chem. Int. Ed. **2013**, 52, 2166-2179.
4. S. Jiang, J. H. ter Horst, Cryst. Growth Des. **2011**, 11, 256-261.
5. S. S. Kadam, S. A. Kulkarni, R. C. Ribera, A. I. Stankiewicz, J. H. ter Horst, H. J. M. Kramer, Chemical Engineering Science **2012,** 72, 10–19.
6. S A. Kulkarni, S. S. Kadam, H. Meekes, A. I. Stankiewicz and J. H. ter Horst, Cryst. Growth Des. **2013,** 13, 2435-2440.
7. R. J. Davey, N. Blagden, S. Righini, H. Alison, M. J. Quayle, and S. Fuller, Cryst. Growth Des. **2001,** 1, 59-65.

8. C. A. Hunter, J. F. McCabe and A.Spitaleri, CrystEngComm, **2012**, 14, 7115-7117.
9. R. J. Davey, G. Dent, R. K. Mughal, and S. Parveen, Cryst. Growth Des. **2006,** 6, 1788-1796.
10. S, A, Kulkarni, E. S. McGarrity, H. Meekes and J. H. ter Horst, Chem. Commun. **2012**, 48, 4983–4985.
11. A. Mattei, X. Mei, A-F Miller and T. Li, Cryst. Growth Des. **2013**, 13, 3303- 3307.
12. R. C. Burton, E. S. Ferrari, R. J. Davey, J. L. Finney, and D. T. Bowron, J. Phys. Chem. B **2010,** 114, 8807–8816.
13. H. Hao, M. Barrett, Y. Hu, W. Su, S. Ferguson, B. Wood and Brian Glennon, Org. Process Res. Dev. **2012**, 16, 35–41.
14. T. F. Lai and R. E. Marsh, Acta Cryst. **1967**, 22, 885- 893.
15. S. Gracin and A. Fischer, Acta Cryst. **2005**, 61, 1242–1244.
16. S. Gracin and Å. C. Rasmuson, Cryst. Growth Des. **2004,** 4, 1013- 1023.
17. G. Bruno and L. Randaccio, Acta Cryst. **1980,** 36, 1711-1712.
18. M. Svärd, F. L. Nordström, E-M Hoffmann, B. Aziz and Å. C. Rasmuson, CrystEngComm. **2013,** 15, 5020-5031.
19. J. Thati, F. L. Nordström and Å. C. Rasmuson, J. Chem. Eng. Data, **2010,** 55, 5124-5127.
20. H. B. Callen, Thermodynamics and An Introduction to Thermostatistics, 2nd ed., John Wiley & Sons, New York, **1985**.
21. M. C. Payne, M. P. Teter, D. C. Allen, T. A. Arias and J. D. Joannopoulos, Rev. Mod. Phys. **1992**, 64, 1045–1097.
22. B. Hess, C. Kutzner, D. Van der Spoel, E. Lindahl, J. Chem. Theory Comput. **2008,** 435- 447.
23. J. Wang, R. M. Wolf, J. W. Caldwell, P. A. Kollman, D. A. Case, J. Chem. Computer. **2004,** 25, 1157- 1174.
24. J. Wang, W. Wang, P. A. Kollman, D. A. Case, Journal of Molecular Graphics and Modelling, **2006,** 25, 247- 260.
25. Wei Du, Personal Communication, **2013.**
26. O. Sohnel and J. Garside, Precipitation: Basic Principles and Industrial Applications, Butterworth Heinemann, Oxford, **1992.**

27. W. J. Dunning and N. T. Notley, Z. Elektrochem. **1957**, 61, 55 – 59.
28. D. I. A Miller, I. D. H Oswalds, D. J Francis, W G Marshall, C. R Pulham, A. S Cunning, Chem. Comm. **2009**, 562-564.

TOC Graphic

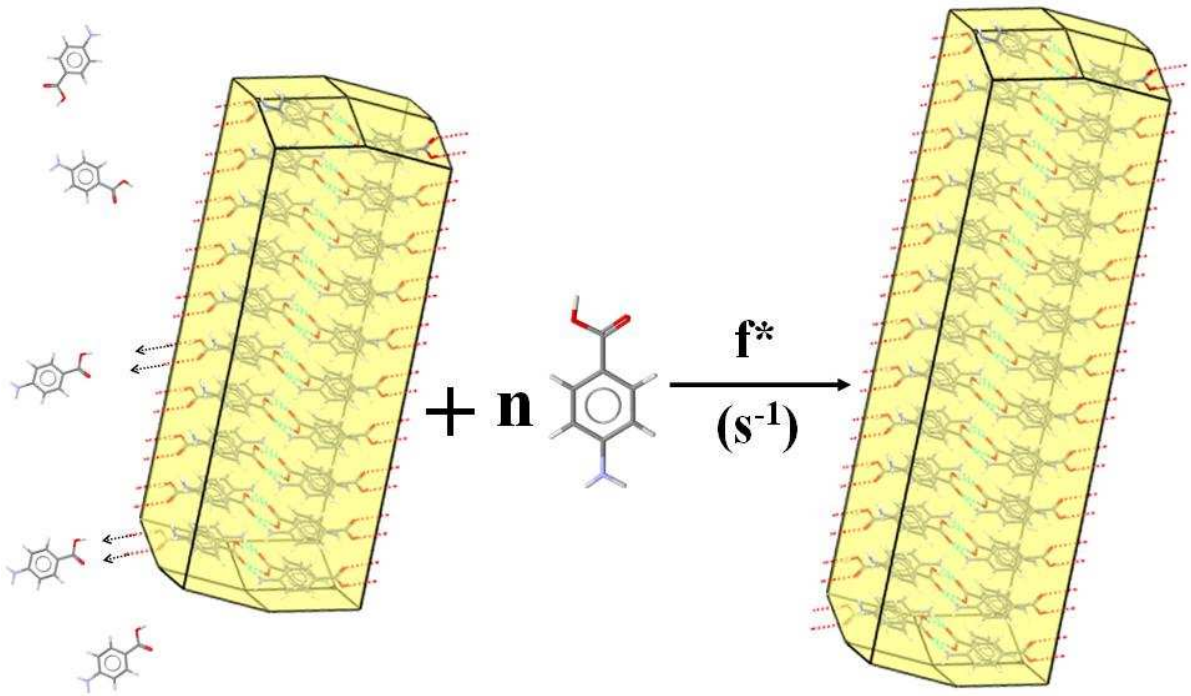
+ n
f*
(s-1)